Thermodynamic entropy generation model for metal fatigue failure

Hossein Salimi[a], Mohammad Pourgol-Mohammad[*a], Mojtaba Yazdani[a]
[a] Sahand University of Technology, Tabriz, Iran

Abstract: Fatigue damage is comprehensively determined by thermodynamic entropy generation as the damage precursor. For fatigue mechanism, time rate of thermodynamic entropy generation is defined as ratio of plastic strain energy density rate per specimen's temperature. Recent researches claim that entropy generation is constant at the time of crack initiation, directly related to the type of material, independent of loading and surrounding conditions. In this study, an analytical solution is proposed to evaluate the temperature of specimen during the fatigue test while the Morrow equation employed as plastic strain energy density. Result leads to derive new analytical-empirical model for calculating entropy generation. It is shown that temperature obtained from analytical solution is in good agreement with experimental data. In the next section, uncertainty and sensitivity analysis are accomplished based on proposed model. Monte-Carlo simulation and sigma-normalized derivative methods are employed for uncertainty and sensitivity analysis, respectively. Specimen's diameter, ambient temperature, loading stress level and frequency are considered as effective independent parameters. Al 2024-T4 used as case study. Analytical-empirical model represents that considered parameters are effective on fatigue fracture entropy (FFE) and the hypothesis of constant entropy generation is generally unacceptable in the crack initiation time.

Keywords: fatigue, thermodynamic entropy generation, crack initiation, uncertainty analysis, sensitivity analysis.

1. INTRODUCTION

Mechanical methods of life estimation and reliability analysis have been unchanged for structures for several years while many researches show existence of significant uncertainties and conservative factors. Thus, it is necessary to study effective methods with capability of more accurate damage behavior prediction. For life estimation of component, the definition and evaluation of damage are very important. Thermodynamically, all damage mechanisms share common feature of energy dissipation. Dissipation is fundamental measure of irreversibility. The irreversibility is quantified in thermodynamic approach by entropy generation estimation [1]. Amiri and Modarres [1] state irreversible phenomena for different mechanical damage mechanisms and Pourgol-Mohammad et al. [2] reviewed present studies in the thermodynamic entropy generation concept for mechanical damage mechanisms. In fatigue process, crack initiation and growth is an irreversible phenomena, therefore, it causes entropy generation in the system [1].

In recent years, several studies are conducted in concept of entropy generation for fatigue mechanism [1-22]. These studies claimed that the value of entropy generation is constant for a specific material at the time of full fracture [3, 8-10, 13, 17]. This constant value is independent of specimen geometry, loading type, applied stress level and loading frequency. In other word, the necessary and sufficient condition for fracture of a specimen is that the entropy generation reaches a specified value named Fracture Fatigue Entropy (FFE) [11]. The hypothesis of constant entropy generation for a specific material at the time of full fracture led to calculation of FFE for different materials as a material property. In this regard, the value of FFE = 60 MJ/m^{3}K for SS 304 [11, 17] and FFE = 25 MJ/m^{3}K for LCS 1018, MCS 1045 and API 5L X52 [8-10] are determined. While, for Al 6061 different values of 8 MJ/m^{3}K [10] and 9 MJ/m^{3}K [8] are calculated. This is in contrast of constant FFE for each material.

Recent researches presented that the most part of fatigue life elapsed up to macro crack initiation [3, 13, 17, 20]. Thus, from the structural reliability viewpoint, there is no sensible difference between specimen that considered up to crack initiation and the other one which has allowed reaching full fracture [20]. Naderi and Khonsari [13, 17] and Amiri et al. [3] state that the crack initiation point is

[*] Email: *pourgolmohammad@sut.ac.ir*

almost about 90% of fatigue life. They also reported that there is almost linear relationship between normalized entropy generation and normalized applied cycle ($\frac{\gamma}{\gamma_f} \cong \frac{N}{N_f}$). Based on hypothesis of constant entropy generation at full fracture time and by considering of 90% fatigue life for crack initiation life, it leads to 0.9 FFE for entropy generation at the time of crack initiation. It means that entropy generation is also constant for a specific material in the crack initiation time. However, Ontiveros et al. [18-20] disputed the concept of constant entropy generation in the crack initiation. They reported that the hypothesis of constant entropy accumulation (or constant energy accumulation) is still valid for fatigue crack initiation and suggested that more studies are needed for the claim to be approved [18]. Yousefi Faal et al. [22] calculated reliability up to the fatigue crack initiation time based on numerical and theoretical analysis and they confirmed Ontiveros report.
In this study, calculation of entropy generation in the crack initiation time is of interest for metal materials. All presented researches are mainly based on experimental basis, while analytical analysis is considered in this study. The entropy generation is determined by calculating specimen temperature while the empirical relations (such as Morrow equation) are employed as plastic strain energy density. A new analytical method proposed for temperature analytical solution and new analytical-empirical model derived for calculating entropy generation in the crack initiation time.

2. THEORETICAL BACKGROUND

Entropy expresses a variation of energy associated with a variation in the temperature [23]. Considering irreversible process, second law of thermodynamic represent [1]:

$$dS = d_e S + d_i S, \qquad d_i S > 0 \tag{1}$$

where d_eS is the entropy exchange (flow) with the surrounding and d_iS is entropy generation inside the system (Figure 1).

Figure 1 Entropy balance in a system [1]

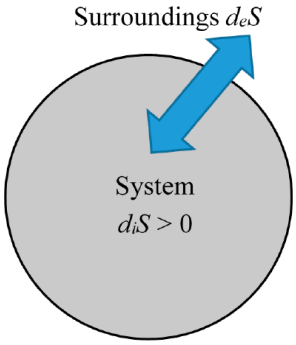

$dS = d_eS + d_iS$

Under the hypothesis of local equilibrium, the entropy balance (Eq. (1)) is expressed in local form as:

$$\rho \frac{ds}{dt} = -\nabla . \mathbf{J}_s + \dot{\gamma} \tag{2}$$

where:

$$S = \int_V \rho s dV \tag{3}$$

$$\frac{d_e S}{dt} = \int_\Omega \mathbf{J}_s . d\mathbf{\Omega} \tag{4}$$

$$\frac{d_i S}{dt} = \int_V \dot{\gamma} dV \tag{5}$$

Here, the symbols are: s the entropy per unit mass, ρ the density, $\mathbf{J}_s$ the total entropy flow per unit area and unit time, d**Ω** the element of surface area (Figure 2), and $\dot{\gamma}$ denotes the entropy generation per unit volume per unit time.

Figure 2 Entropy Generation and Entropy Flow for a System [1]

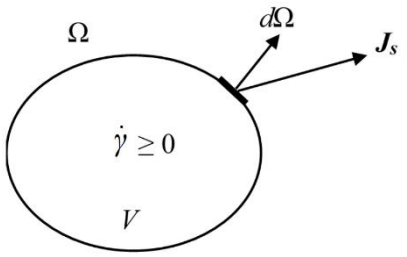

The Clausius–Duhem inequality states that all the deformations cause positive entropy generation rate in solids with internal friction [23]:

$$\dot{\gamma} = \frac{1}{T}\left(\boldsymbol{\sigma} : \dot{\boldsymbol{\varepsilon}}^{\mathbf{p}} - A_k \dot{V}_k - \frac{\mathbf{q}}{T}.\nabla \mathbf{T} \right) \geq 0 \tag{6}$$

where $\dot{\gamma}$ is the time rate of entropy generation, and $\boldsymbol{\sigma}$, $\dot{\boldsymbol{\varepsilon}}^{\mathbf{p}}$, A_k, $\dot{V}_k$, T and $\mathbf{q}$ are stress tensor, rate of plastic strain, thermodynamic forces related to internal variables, internal variable evolution, temperature and vector of thermal gradation, respectively. Subscribe of k denotes number of internal variables [23].

Entropy generation in Eq. (6) has three dissipated terms: plastic dissipation ($\boldsymbol{\sigma} : \dot{\boldsymbol{\varepsilon}}^{\mathbf{p}}$), dissipation related to internal variables ($A_k \dot{V}_k$) and thermal dissipation due to conduction ($\frac{\mathbf{q}.\nabla \mathbf{T}}{T}$) [24]. $A_k \dot{V}_k$ represents the nonrecoverable energy stored in the material. For metals, this is the energy of the field of the residual micro stresses, accompanying the increase in the dislocation density. It represents only 5-10% of the term $\boldsymbol{\sigma} : \dot{\boldsymbol{\varepsilon}}^{\mathbf{p}}$ and is often negligible [23] so:

$$A_k \dot{V}_k \approx 0 \tag{7}$$

In processes involving low-cycle fatigue, the entropy generation due to plastic deformation is dominant and the entropy generation is negligible due to heat conduction. The corresponding entropy generation starts slowly and it grows while the entropy generation due to plastic deformation remains to be dominant throughout the process. Therefore, Eq. (6) reduces to [13]:

$$\dot{\gamma} = \frac{1}{T}\left(\boldsymbol{\sigma} : \dot{\boldsymbol{\varepsilon}}^{\mathbf{p}} \right) = \frac{\dot{W}_p}{T} \tag{8}$$

Therefore, the total entropy generation can be obtained by integration of Eq. (8) up to the time t_f when macro crack initiation occurs:

$$\gamma_f = \int_0^{t_f} \frac{\dot{W}_p}{T} dt \tag{9}$$

where γ_f is the total entropy generation at the onset of macro crack initiation.

Heat equation for fatigue mechanism presented as [23]:

$$k \nabla^2 T = \rho C \dot{T} - \boldsymbol{\sigma} : \dot{\boldsymbol{\varepsilon}}^{\mathbf{p}} - T \frac{\partial \boldsymbol{\sigma}}{\partial T} : \dot{\boldsymbol{\varepsilon}}^{\mathbf{e}} \tag{10}$$

where ∇^2 denotes Laplacian operator and C is Specific Heat Capacity of material. Eq. (10) indicates balance between 4 terms: Conductivity heat transfer ($k \nabla^2 T$), retardation effect because of heat inertia ($\rho C \dot{T}$), internal heat generation due to plastic deformation ($\boldsymbol{\sigma} : \dot{\boldsymbol{\varepsilon}}^{\mathbf{p}}$), which is responsible for increase in mean temperature, and thermoelastic coupling term ($T \frac{\partial \boldsymbol{\sigma}}{\partial T} : \dot{\boldsymbol{\varepsilon}}^{\mathbf{e}}$) [11]. Temperature fluctuation due to thermoelastic coupling is small in comparison with the mean temperature and it is neglectable [25]:

$$\rho C \dot{T} - k \nabla^2 T = \dot{W}_p \tag{11}$$

In Eq. (11) plastic strain energy density affect as thermal source which is uniformly distributed in specimen's gage section [26]. Figure 3 presents typical evolution of temperature during fatigue test. For stresses more than fatigue endurance, there is 3 phase in Figure 3. Phase 1 (initial phase) which temperature is gradually raised and that has greater initial slope for higher stress level. Phase 2 (steady state) which there is balance between generated hysteresis energy and dissipated heat energy. Phase 3 (crack initiation phase) which temperature suddenly increased before final rupture [26].

Figure 3 Typical temperature evolution for a fatigue test [3]

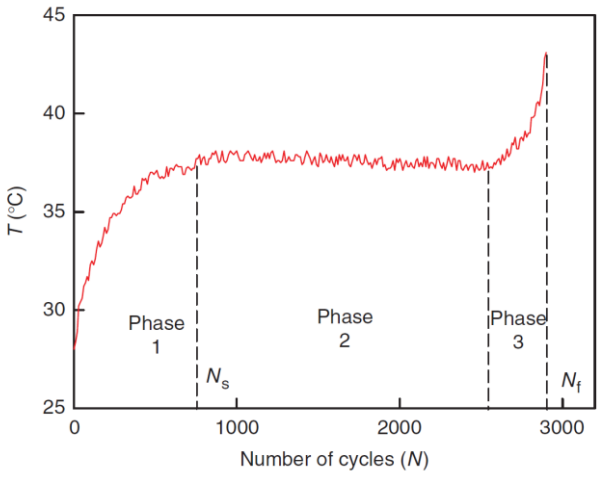

3. ANALYTICAL SOLUTION

Figure 4 presents schematic shape of specimens in fatigue test (ASTM E466 and ASTM E606). They could have rectangular or round cross section.

Figure 4 Schematic shape of fatigue test specimens [27, 28]

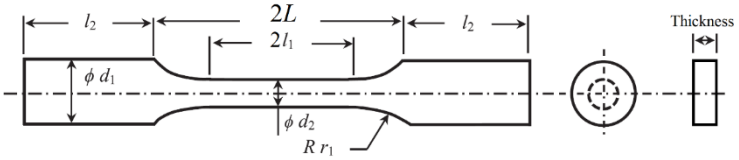

In these specimens, parts with larger cross section area (parts with l_2 length at the end of specimen) be hold in testing machine grip. A sample of fatigue test setup presented in Figure 5.

Figure 5 A fatigue test setup for uniaxial loading [8]

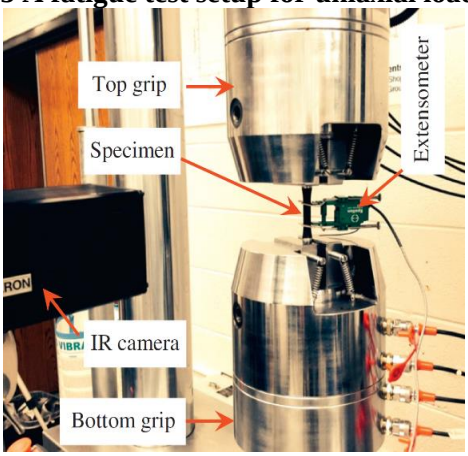

Testing machine grip due to larger volume in comparison with specimen's end section act like a heat sink. Because of high conductivity of metal specimens, the end section of specimens which are in contact with testing machine grip could be considered as constant temperature in equilibrium with grip temperature (T_∞). Experimental result confirms this assumption (Figure 6). Therefore, temperature gradient occurs in middle section of specimen (section with 2L length). In this middle section, plastic strain energy act on gage section (section with $2l_1$ length) and the rest section (section between l_1 and L) is stable. In metallic material that usually adopted in engineering structures the heat transfer capacity by convection is much lower than the heat transfer capacity by conduction and therefore, the

temperature variation in the specimen cross section can be neglected. This fact is demonstrated by the very low Biot numbers (much lower than 1) that can be calculated for specimens which commonly used in fatigue tests [25].

Figure 6 Temperature contour in a) MCS 1045 in 55% of fatigue life under low cycle fatigue with σ_{max} = 500 MPa, frequency 10 Hz and load ratio of -0.6 [8], b) ULTIMET super alloy in 95640 (left) and 95520 cycle (right) under high cycle fatigue with σ_{max} = 700 MPa, frequency 20 Hz and load ratio of 0.05 [26]

(a) (b)

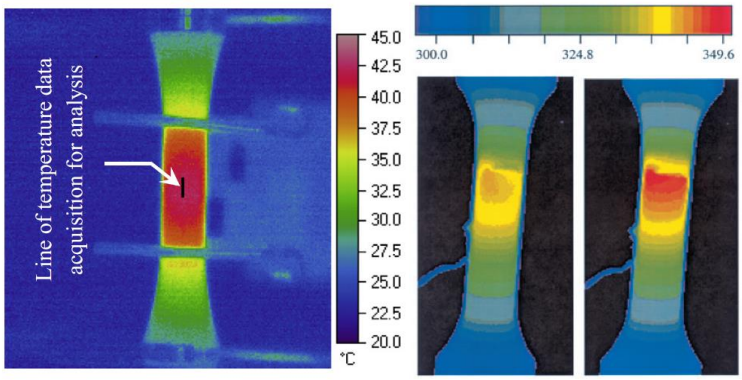

Therefore, heat equation and boundary and initial conditions (Figure 7) becomes:

$$\rho C\dot{T} - k\frac{\partial^2 T}{\partial x^2} = \dot{W}_p \tag{12}$$

$$\frac{\partial T}{\partial x}(0,t) = 0 \tag{13}$$

$$T(L,t) = T_\infty$$

$$T(x,0) = T_i = T_\infty \tag{14}$$

Figure 7 Boundary conditions with 1-dimensional heat transfer assumption

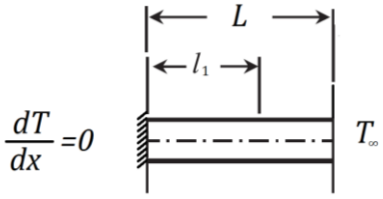

Before expression of analytical solution for Eq. (12) with boundary and initial conditions of (13) and (14), let us consider second phase of temperature evolution (Figure 3). In this phase which is the most part of fatigue life, temperature is in steady state:

$$\dot{T} = 0 \tag{15}$$

Therefore Eq. (12) becomes:

$$\frac{d^2 T}{dx^2} = -\frac{\dot{W}_p}{k} \tag{16}$$

For very simple case of $\frac{l_1}{L} \approx 1$ Eq. (16) results:

$$T(x) = -\frac{\dot{W}_p}{2k}x^2 + C_1 x + C_2, \quad \frac{dT}{dx}(x=0) = 0, \quad T(x=L) = T_\infty$$

$$T(x) = \frac{\dot{W}_p}{2k}\left(L^2 - x^2\right) + T_\infty \tag{17}$$

By utilizing Fourier law, heat transfer by conductivity at each point of x becomes:

$$q''_{Cond}(x) = -kA\frac{dT}{dx} = A\dot{W}_p x \tag{18}$$

As result, the heat transfer at the end of specimen becomes:

$$q''_{Cond}(x = L) = A\dot{W}_p L \tag{19}$$

By considering:

$$q''_{Cond} = \frac{\Delta T}{R}, \quad R = \frac{L_c}{kA} \tag{20}$$

where R is heat resistance and L_c is effective length, results:

$$\Delta T\big|_{x=L} = T_0 - T_\infty = \frac{\dot{W}_p L^2}{2k}, \quad q''_{Cond}\big|_{x=L} = \frac{kA}{L_c}\times\frac{\dot{W}_p L^2}{2k} = \dot{W}_p A\frac{L^2}{2L_c} \quad \Rightarrow \quad L_c = \frac{L}{2} \tag{21}$$

This means for specimens with uniform internal heat source, we can used Eq. (20) for heat transfer amount at the end of specimen while effective length of specimen was considered as L/2.

For $\frac{l_1}{L} \neq 1$ we need to calculate effective length. In this condition and for section with no internal heat source, because of energy stability we have (Figure 8):

$$q''_{Cond} = q''_{Cond\,1} \tag{22}$$

Figure 8 Heat balance in fatigue specimen

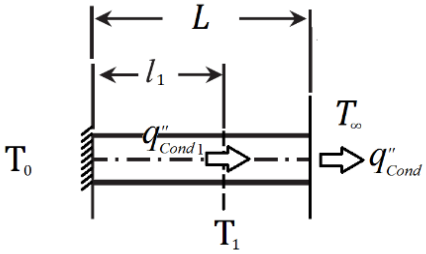

Eq. (22) results:

$$kA\frac{\Delta T}{L_c} = kA\frac{\Delta T_1}{L_{c1}} \quad \Rightarrow \quad kA\frac{T_0 - T_\infty}{L_c} = 2kA\frac{T_0 - T_1}{l_1} \quad \Rightarrow \quad L_c = \frac{l_1}{2}\times\frac{T_0 - T_\infty}{T_0 - T_1} \tag{23}$$

In Eq. (23) term of T_1 appears that needs to be removed. By considering heat balance for section with no internal heat source (Figure 9):

$$q''_{Cond\,1} = q''_{Cond\,2} \tag{24}$$

Figure 9 Heat balance in section with no internal heat source

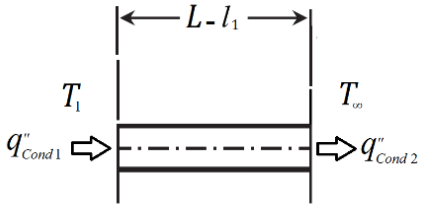

which leads:

$$kA\frac{\Delta T_1}{L_{c1}} = kA\frac{\Delta T_2}{L_{c2}} \quad \Rightarrow \quad 2kA\frac{T_0 - T_1}{l_1} = kA\frac{T_1 - T_\infty}{L - l_1} \quad \Rightarrow \quad T_1 = \frac{l_1}{2L - l_1}\left[\frac{2(L - l_1)}{l_1}T_0 + T_\infty\right] \tag{25}$$

By substituting Eq. (25) in Eq. (23) we have:

$$L_c = \frac{2L - l_1}{2} \tag{26}$$

Therefore, heat transfer at the end of specimen becomes:

$$R = \frac{2L - l_1}{2kA} \tag{27}$$

$$q''_{Cond} = \frac{T_0 - T_\infty}{R} = 2kA\frac{T_0 - T_\infty}{2L - l_1} \tag{28}$$

Metallic material that adopted in fatigue test usually have high thermal conductivity (k) and short length (L) which results small heat resistance (R) and therefore it can be assumed that heat transfer to the grip at the end of specimen at any instant is:

$$q''_{Cond}(t) = 2kA\frac{T(t)-T_\infty}{2L-l_1} \tag{29}$$

Integration of Eq. (12) on control volume and applying boundary conditions results:

$$\int_{V'=Al_1} \dot{W}_p dV = \int_{V=LA} \rho C\frac{\partial T}{\partial t}dV - \int_{S_{cd}} k\frac{\partial T}{\partial x}.ndS - \int_{S_{cv}} h(T-T_\infty)dS_{cv} - \int_{S_{ir}} \kappa\sigma_n\left(T^4-T_\infty^4\right)dS_{ir} \tag{30}$$

where h is convection heat transfer coefficient, κ surface emissivity, σ_n Stephan-Boltzmann constant which is equal to $5.67\times10^{-8}\frac{W}{m^2K^4}$ and S_{cd}, S_{cv} and S_{ir} are conduction, convection and radiation surfaces, respectively. As mentioned before in metallic specimens the heat transfer by conduction is major heat dissipation mechanism and the other two terms could be neglected. By substituting Eq. (29) in Eq. (30) becomes:

$$\rho VC\frac{dT(t)}{dt} - \frac{T(t)-T_\infty}{R} = V'\dot{W}_p \tag{31}$$

In 1965 Morrow proposed that the plastic strain energy density per cycle was relativity constant throughout the fatigue life and for constant loading conditions under a fully reversed fatigue loads, plastic strain density could be presented as [29-31]:

$$\frac{dW_p}{dN} = 4\sigma'_f\varepsilon'_f\left(\frac{1-n'}{1+n'}\right)(2N_f)^{b+c} \tag{32}$$

where σ'_f is fatigue strength coefficient, b fatigue strength exponent, ε'_f fatigue ductility coefficient, c fatigue ductility exponent, n' cyclic strain hardening exponent and N_f final number of cycles. Another equation that relates fatigue life to stress amplitude (σ_a) separately proposed by L. F. Coffin and S. S. Manson which generally called Coffin-Manson relationship [32, 33]:

$$\sigma_a = \sigma'_f(2N_f)^b \tag{33}$$

By considering Morrow equation as plastic strain density and solving differential equation of (31), specimen's temperature at midpoint becomes:

$$\dot{W}_p = \frac{dW_p}{dN}f = C_1 \quad\Rightarrow\quad T(t) = T_\infty + \frac{V'C_1\beta}{\rho VC} + e^{-\frac{t}{\beta}}\left[(T_i-T_\infty) - \frac{V'C_1\beta}{\rho VC}\right], \quad \beta = \frac{\rho VC}{2kA}(2L-l_1) \tag{34}$$

where f is loading frequency.

By substituting Equations (32) and (34) in Eq. (9) we have:

$$\gamma_f = \frac{\dot{W}_p}{\alpha}\left\{\beta\ln\left[\frac{\alpha}{T_i}\left(1-e^{-t_f/\beta}\right)+e^{-t_f/\beta}\right]+t_f\right\}, \quad \alpha = T_\infty + \frac{\dot{W}_pV'L_c}{kA}, \quad t_f = \frac{N_f}{f} \tag{35}$$

3.1. Validation

Figure 10 shows the temperature evolution up to crack initiation time calculated from analytical solution and experimental data measured by Jiang et al. [26].

Figure 10 The temperature evolution obtained from experimental and analytical solution for σ_a = 703 MPa and 762 MPa.

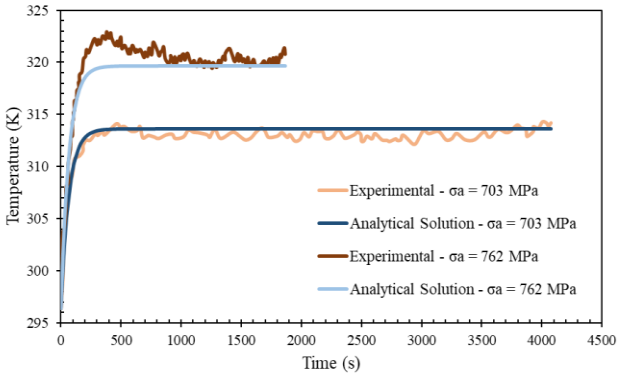

Figure 10 represents that the analytical results are in very good agreement with experimental data.

4. CASE STUDY

As a case study, two fatigue regime (Low Cycle Fatigue and High Cycle Fatigue) are considered separately. For both analysis Aluminum 2024-T4 is used which has common use in airframe constructions. Table 1 and Table 2 represent the physical, mechanical and thermal property and the fatigue property of Al 2024-T4, respectively.

Table 1 The physical, mechanical and thermal properties of Al 2024-T4 [34]

ρ (Kg/m^3)	S_y (MPa)	S_{ut} (MPa)	S_e (MPa)	k (W/m.K)	C (W/Kg.K)
2780	324	469	138	121	875

Table 2 The fatigue properties of Al 2024-T4 [35]

σ'_f (MPa)	ε'_f	b	c	n'
1294	0.327	-0.142	-0.645	0.08

Figure 11 shows the schematic of low cycle fatigue and high cycle fatigue specimens. These specimens are based on ASTM E606 and ASTM E466 standards. Middle part cross section diameter selected as d = 7mm for LCF and d = 15 mm for HCF.

Figure 11 Schematic of specimen for a) LCF, b) HCF [27, 28]

(a) (b)

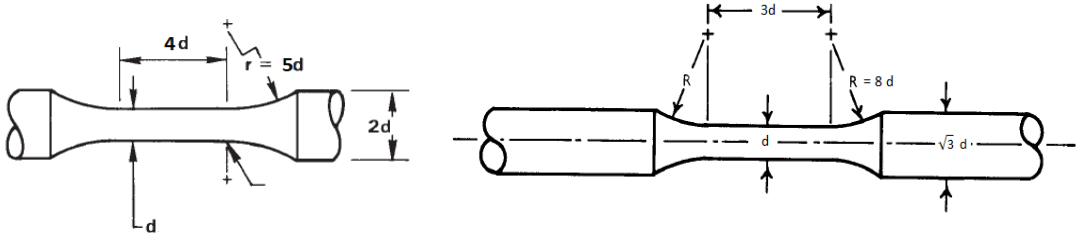

Loading condition was selected as constant amplitude loading under a fully reversed fatigue loads with loading frequency of f = 2.75 Hz and six different applied stress levels (σ_a = 325, 350, 375, 400, 425 and 450 MPa) for LCF and f = 55 Hz and seven different stress level selected (σ_a = 150, 175, 200, 225, 250, 275 and 300 MPa) for HCF. Initial temperature was equal to ambient temperature and that was 296.37 K. Figure 12 presents Fatigue Failure Entropy (FFE) for different fatigue life in LCF and HCF.

Figure 12 Fatigue Failure Entropy (FFE) for different fatigue life in a) LCF, b) HCF

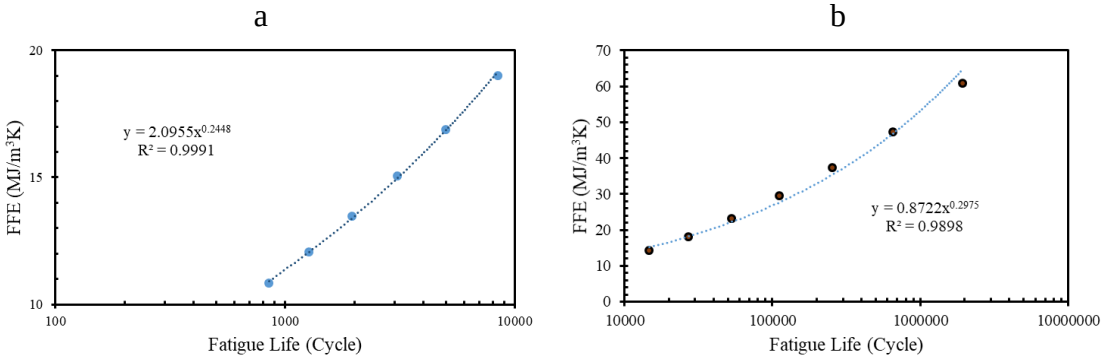

It is evident that for both LCF and HCF regimes FFE is greater for higher fatigue life. In the other words low applying stress results higher FFE.

5. UNCERTAINTY ANALYSIS

For uncertainty analysis, parameter uncertainty is performed based on Eq. (35) and accuracy of measurement equipment such as load cell (±1%) and IR sensor (±1.5% ± 2 K) employed as uncertainty of input variables. For this purpose, input variables are assumed in form of a normal distribution, and Monte Carlo simulation is used to propagate their uncertainties throughout the model. Since almost all mechanical properties in engineering structures are obeyed normal distribution. However, goodness of fit test would be employed for the better fit to the available data. The convergence of Monte Carlo simulation is achieved in 10000 repetitions. Table 3 and Table 4 present the mean and standard deviation of input parameters in LCF and HCF regimes, respectively. In Table 4 variables with similar quantity to Table 3 are avoided.

Table 3 Uncertainty parameters of input variables in LCF

Parameter	**Normal Distribution Parameters (Mean, STD)**
Frequency	f = N (2.75, 0.0275) Hz
Ambient Temperature	T_∞ = N (296.37, 6.445) K
Amplitude Stress level	σ_1 = N (325, 3.25), σ_2 = N (350, 3.5), σ_3 = N (375, 3.75), σ_4 = N (400, 4.0), σ_5 = N (425, 4.25), σ_6 = N (450, 4.5) MPa
Density	ρ = N (2780, 27.8) Kg/m^3
Thermal Properties	C = N (875, 8.75) W/Kg.K, k = N (121, 1.21) W/m.K
Fatigue Properties	σ'_f = N (1294, 12.94) MPa, ε'_f = N (0.327, 0.00327), b = N (-0.142, 0.00142), c = N (-0.645, 0.00645), n' = N (0.08, 0.0008)

Table 4 Uncertainty parameters of input variables in HCF

Parameter	**Normal Distribution Parameters (Mean, STD)**
Frequency	f = N (55, 0.55) Hz
Amplitude Stress level	σ_1 = N (150, 1.5), σ_2 = N (175, 1.75), σ_3 = N (200, 2.0), σ_4 = N (225, 2.25), σ_5 = N (250, 2.5), σ_6 = N (275, 2.75), σ_7 = N (300, 3.0) MPa

Figure 13 a and b present the uncertainty quantification result for difference stress level in LCF and HCF, respectively. In these figures the standard deviation (measure of uncertainty) are plotted versus fatigue test time. It is shown that uncertainty is increased by fatigue cycle increment and the uncertainty growth is more significant for high stress level. This is because of uncertainty accumulation.

Figure 13 Input uncertainty growth throughout model for a) LCF, b) HCF

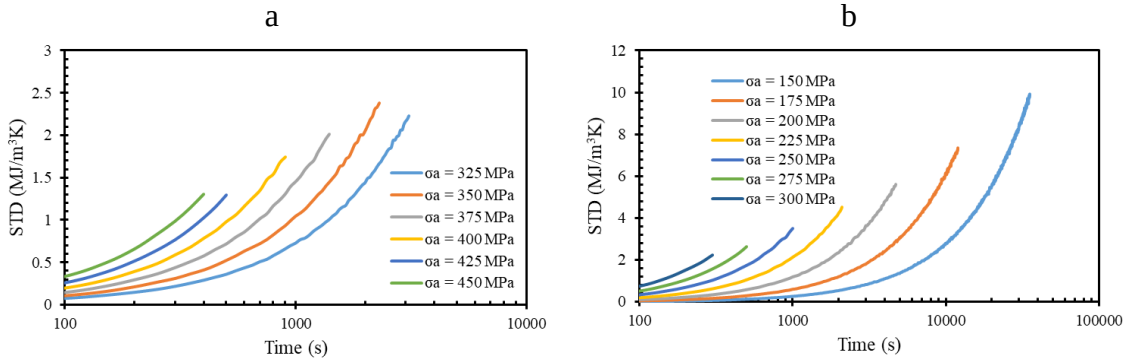

6. SENSITIVITY ANALYSIS

As mentioned before, Figure 13 presents FFE in the crack initiation time is not constant and could not considered as material property. Therefore, sensitivity analysis and investigation of more effective parameter on FFE are needful. In this section sensitivity analysis is performed for both LCF and HCF based on different operation conditions. At first, differential method employed for sensitivity analysis and in the next part based on common selection range for input variables, Sigma-normalized derivative method is used. This method considers usual range for input variables and presents a measure for rank the input variables.

6.1. Differential method

Table 5 presents sensitivity analysis result for LCF in operation condition of d = 7 mm, f = 2.75 Hz, T_∞ = 296.37 K and σ_a = 387.5 MPa and for HCF d = 15 mm, f = 55 Hz, T_∞ = 296.37 K and σ_a = 225 MPa. It is worth noting these conditions selected according to standards constrains, usual conditions in laboratory and loading limits in each fatigue regime (LCF and HCF).

Table 5 Sensitivity analysis based on differential method for LCF and HCF

Input variable (Z_i)	$\frac{\partial \gamma_f}{\partial Z_i}$ for LCF (MJ/m³.K)	$\frac{\partial \gamma_f}{\partial Z_i}$ for HCF (MJ/m³.K)
Diameter (d)	-0.1632 (-1.15%)	-0.4672 (-1.59%)
Frequency (f)	-0.2078 (-1.46%)	-0.0637 (-0.22%)
Ambient Temperature (T_∞)	-0.0461 (-0.32%)	-0.0871 (-0.30%)
Amplitude Stress (σ_a)	-0.0633 (-0.44%)	-0.2817 (-0.96%)

As it is recognizable almost all of the 4 parameters are effective on FFE and FFE is sensitive to all four parameters. This method states ambient temperature and loading frequency have lowest effect on FFE for LCF and HCF, respectively.

6.2. Sigma-normalized derivative method

Standards, testing equipment limitation, laboratory conditions, testing constrains and some other factors cause fatigue variables are selected in specific ranges which these ranges could be different for LCF and HCF. For example, ASTM E466 limits selection range of specimen's midsection diameter to 5.08 up to 25.4 mm, or for LCF applied stress level must be more than yield stress and less than ultimate stress. Therefore, Sigma-normalized derivative method employed to sensitivity analysis for LCF and HCF. Normal distribution assumed for selecting operation point and Monte Carlo simulation used to calculate dispersion of model output.
Sigma-normalized derivative measure defines as [36]:

$$S_{Z_i} = \frac{\sigma_{Z_i} \partial \gamma_f}{\sigma_{\gamma_f} \partial Z_i} \tag{36}$$

where σ_{Z_i} and σ_{γ_f} are standard deviation of input variables and model, respectively. Table 6 presents mean and standard deviation of each input variable for LCF and HCF.

Table 6 Normal distribution parameters of each input variable for LCF and HCF

Input variable (Z_i)	Normal Distribution Parameters (Mean, STD) for LCF	Normal Distribution Parameters (Mean, STD) for HCF
Diameter (d)	d = N(7, 1) mm	d = N(15, 3.33) mm
Frequency (f)	f = N(2.75, 0.75)Hz	f = N(55, 15)Hz
Ambient Temperature (T_∞)	T_∞ = N(296.37, 5) K	T_∞ = N(296.37, 5) K
Amplitude Stress (σ_a)	σ_a = N(387.5, 20.83) MPa	σ_a = N(225, 25) MPa

Monte Carlo simulation calculates 14.2384 MJ/m^{3}K for mean value and 1.3766 MJ/m^{3}K for standard deviation of FFE in LCF. Similarly, 29.4238 and 7.6213 MJ/m^{3}K are calculated as mean value and standard deviation of FFE in HCF, respectively. Results of Sigma-normalized derivative sensitivity analysis present in Table 7 for LCF and HCF.

Table 7 Sensitivity analysis based on Sigma-normalized derivative method for LCF and HCF

Input variable (Z_i)	S_{Z_i} for LCF	S_{Z_i} for HCF
Diameter (d)	-0.11855095	-0.204338399
Frequency (f)	-0.113211799	-0.12537158
Ambient Temperature (T_∞)	-0.167438688	-0.057142149
Amplitude Stress (σ_a)	-0.957958426	-0.924049557

As it is recognizable from Table 7 in LCF all of the four input variables are effective on FFE. However, in HCF FFE almost is not sensitive to ambient temperature. Therefore, ambient temperature has low corporation in FFE and is not important factor for HCF regime. For both LCF and HCF amplitude stress level is the most important factor and FFE is the most sensitive to amplitude stress level.

7. CONCLUSION

In this study, hypothesis of constant entropy generation is investigated at the time of crack initiation in fatigue process. For this purpose, a new analytical solution is carried out to evaluate the temperature of specimen during the test while the common empirical relation (e.g., Morrow equation) is employed as plastic strain energy density. Result leads to derive new analytical-empirical model for calculating entropy generation at the time of crack initiation. It is shown that temperature obtained from analytical solution is in good agreement with experimental data. In the next section, uncertainty and sensitivity analysis accomplished based on proposed model. Monte-Carlo simulation is employed for uncertainty analysis. Sensitivity analysis performed using differential and Sigma-normalized derivative methods. Several factors such as specimen's diameter, ambient temperature, loading stress and frequency are considered as effective independent parameters. Al 2024-T4 used as case study.

Analytical-empirical model represents that considered parameters are effective on fatigue fracture entropy (FFE) and the hypothesis of constant entropy generation is generally unacceptable in the crack initiation time and it cannot be assumed that it is only related to the type of material. Sensitivity analysis shows in LCF all of these four parameters are effective on FFE. However, in HCF between these parameters, ambient temperature has low effect on FFE and FFE is not sensitive on that. For both LCF and HCF amplitude stress level is the most important factor and FFE is the most sensitive to amplitude stress level. Also observed that other parameters were important and could not be ignored.

References

[1] M. Amiri, M. Modarres, "*An entropy-based damage characterization*", *Entropy*, Vol. 16, No. 12, pp. 6434-6463, (2014).

[2] M. Pourgol-Mohammad, H. Salimi, A. Moharrami, "*A Review of Thermodynamic Entropy-Based Damage Determination"*, in *5th International Reliability and Safety Engineering Conference (IRSEC 2018)*, Shiraz, (2018).
[3] M. Amiri, M. Naderi, M. M. Khonsari, "*An experimental approach to evaluate the critical damage*", *International Journal of Damage Mechanics*, Vol. 20, No. 1, pp. 89-112, (2011).
[4] A. Imanian, M. Modarres, "*A thermodynamic entropy-based damage assessment with applications to prognostics and health management*", *Structural Health Monitoring*, (2017).
[5] A. Imanian, M. Modarres, "*A thermodynamic entropy approach to reliability assessment with applications to corrosion fatigue*", *Entropy*, Vol. 17, No. 10, pp. 6995-7020, (2015).
[6] Y. F. Ital'yantsev, "*Thermodynamic state of deformed solids. Report 1. Determination of local functions of state*", *Strength of Materials*, Vol. 16, No. 2, pp. 238-241, (1984).
[7] Y. F. Ital'yantsev, "*Thermodynamic state of deformed solids. Report 2. Entropy failure criteria and their application for simple tensile loading problems*", *Strength of Materials*, Vol. 16, No. 2, pp. 242-247, (1984).
[8] M. Liakat, M. Khonsari, "*Entropic characterization of metal fatigue with stress concentration*", *International Journal of Fatigue*, Vol. 70, pp. 223-234, (2015).
[9] M. Liakat, M. Khonsari, "*On the anelasticity and fatigue fracture entropy in high-cycle metal fatigue*", *Materials & Design*, Vol. 82, pp. 18-27, (2015).
[10] M. Liakat, M. Khonsari, "*Rapid estimation of fatigue entropy and toughness in metals*", *Materials & Design (1980-2015)*, Vol. 62, pp. 149-157, (2014).
[11] M. Naderi, M. Amiri, M. Khonsari, "*On the thermodynamic entropy of fatigue fracture"*, in *Proceeding of*, The Royal Society, pp. 423-438, (2010).
[12] M. Naderi, M. Khonsari, "*A comprehensive fatigue failure criterion based on thermodynamic approach*", *Journal of Composite Materials*, Vol. 46, No. 4, pp. 437-447, (2012).
[13] M. Naderi, M. Khonsari, "*An experimental approach to low-cycle fatigue damage based on thermodynamic entropy*", *International Journal of Solids and Structures*, Vol. 47, No. 6, pp. 875-880, (2010).
[14] M. Naderi, M. Khonsari, "*On the role of damage energy in the fatigue degradation characterization of a composite laminate*", *Composites Part B: Engineering*, Vol. 45, No. 1, pp. 528-537, (2013).
[15] M. Naderi, M. Khonsari, "*Real-time fatigue life monitoring based on thermodynamic entropy*", *Structural health monitoring*, Vol. 10, No. 2, pp. 189-197, (2011).
[16] M. Naderi, M. Khonsari, "*Thermodynamic analysis of fatigue failure in a composite laminate*", *Mechanics of Materials*, Vol. 46, pp. 113-122, (2012).
[17] M. Naderi, M. Khonsari, "*A thermodynamic approach to fatigue damage accumulation under variable loading*", *Materials Science and Engineering: A*, Vol. 527, No. 23, pp. 6133-6139, (2010).
[18] V. Ontiveros, M. Amiri, A. Kahirdeh, M. Modarres, "*Thermodynamic entropy generation in the course of the fatigue crack initiation*", *Fatigue & Fracture of Engineering Materials & Structures*, Vol. 40, No. 3, pp. 423-434, (2017).
[19] V. Ontiveros, M. Amiri, M. Modarres, "*Fatigue crack initiation assessment based on thermodynamic entropy generation*", *Proc. Inst. Mech. Eng. C J. Mech. Eng. Sci*, (2014).
[20] V. L. Ontiveros, M. Modarres, M. Amiri, "*Estimation of reliability of structures subject to fatigue loading using plastic strain energy and thermodynamic entropy generation*", *Proceedings of the Institution of Mechanical Engineers, Part O: Journal of Risk and Reliability*, Vol. 229, No. 3, pp. 220-236, (2015).
[21] P. Whaley, P. Chen, G. Smith, "*Continuous measurement of material damping during fatigue tests*", *Experimental mechanics*, Vol. 24, No. 4, pp. 342-348, (1984).
[22] M. Yousefi Faal, H. Salimi, M. Pourgol-Mohammad, R. Khoshbakhti Saray, "*LIFE ASSESSMENT BASED ON NUMERICAL THERMODYNAMIC ENTROPY ESTIMATION; CASE STUDY OF METAL FATIGUE"*, in *International Mechanical Engineering Congress and Exposition IMECE2017*, Tampa, Florida, USA, (2017).
[23] J. Lemaitre, J.-L. Chaboche, "*Mechanics of solid materials"*: Cambridge university press, 1994,
[24] M. Amiri, M. M. Khonsari, "*On the role of entropy generation in processes involving fatigue*", *Entropy*, Vol. 14, No. 1, pp. 24-31, (2011).
[25] G. Meneghetti, "*Analysis of the fatigue strength of a stainless steel based on the energy dissipation*", *International journal of fatigue*, Vol. 29, No. 1, pp. 81-94, (2007).

[26] L. Jiang, H. Wang, P. Liaw, C. Brooks, D. Klarstrom, "*Characterization of the temperature evolution during high-cycle fatigue of the ULTIMET superalloy: experiment and theoretical modeling*", *Metallurgical and Materials Transactions A*, Vol. 32, No. 9, pp. 2279-2296, (2001).
[27] A. Standard, "*E466: Standard Practice for Conduction Force Controlled Constant Amplitude Axial Fatigue Test of Metallic Materials, vol. 03.01*", *Annual Book of ASTM Standards, West Conshohocken*, (2002).
[28] A. Standard, "*E606-92*", *Standard Practice for Strain-Controlled Fatigue Testing," Annual Book of ASTM Standards*, Vol. 3, (2004).
[29] J. Morrow, *"Cyclic plastic strain energy and fatigue of metals*", in: *Internal friction, damping, and cyclic plasticity*, Eds.: ASTM International, 1965.
[30] G. Halford, "*The energy required for fatigue(Plastic strain hystersis energy required for fatigue in ferrous and nonferrous metals)*", *Journal of materials*, Vol. 1, pp. 3-18, (1966).
[31] J. Park, D. Nelson, "*Evaluation of an energy-based approach and a critical plane approach for predicting constant amplitude multiaxial fatigue life*", *International Journal of Fatigue*, Vol. 22, No. 1, pp. 23-39, (2000).
[32] L. Coffin, "*The stability of metals under cyclic plastic strain*", *Journal of Basic Engineering*, Vol. 82, No. 3, pp. 671-682, (1960).
[33] S. Manson, "*Interpretive report on cumulative fatigue damage in the low cycle range*", (1964).
[34] M. Bauccio, "*ASM metals reference book"*: ASM international, 1993.
[35] N. E. Dowling, "*Mechanical behavior of materials*", 2012.
[36] A. Saltelli, M. Ratto, T. Andres, F. Campolongo, J. Cariboni, D. Gatelli, M. Saisana, S. Tarantola, "*Global sensitivity analysis: the primer"*: John Wiley & Sons, 2008.